Published in final edited form as:
Mol Cancer Ther. 2013 October ; 12(10): 1994–2005. doi:10.1158/1535-7163.MCT-13-0206.

The dual pathway inhibitor rigosertib is effective in direct-patient tumor xenografts of head and neck squamous cell carcinomas

Ryan T. Anderson[1,*], **Stephen B. Keysar**[1,*], **Daniel W. Bowles**[1], **Magdalena J. Glogowska**[1], **David P. Astling**[1], **J. Jason Morton**[1], **Phuong Le**[1], **Adrian Umpierrez**[1], **Justin Eagles-Soukup**[1], **Gregory N. Gan**[2], **Brian W. Vogler**[1], **Daniel Sehrt**[1], **Sarah M. Takimoto**[1], **Dara L. Aisner**[3], **Francois Wilhelm**[4], **Barbara A. Frederick**[2], **Marileila Varella-Garcia**[1], **Aik-Choon Tan**[1], and **Antonio Jimeno**[1]

[1]Division of Medical Oncology, Department of Medicine, University of Colorado School of Medicine, Aurora, CO

[2]Department of Radiation Oncology, University of Colorado School of Medicine

[3]Department of Pathology, University of Colorado School of Medicine

[4]Onconova Therapeutics, Inc., Newtown, PA

Abstract

The dual pathway inhibitor rigosertib inhibits phosphoinositide 3-kinase (PI3K) pathway activation as well as polo-like kinase 1 (PLK1) activity across a broad spectrum of cancer cell lines. The importance of *PIK3CA* alterations in head and neck squamous cell cancer (HNSCC) has raised interest in exploring agents targeting PI3K, the product of PIK3CA. The genetic and molecular basis of rigosertib treatment response was investigated in a panel of 16 HNSCC cell lines, and direct patient tumor xenografts from 8 HNSCC patients (4 HPV16-positive). HNSCC cell lines and xenografts were characterized by pathway enrichment gene expression analysis, exon sequencing, gene copy number, western blotting, and IHC. Rigosertib had potent antiproliferative effects on 11 of the 16 HPV− HNSCC cell lines. Treatment sensitivity was confirmed in two cell lines using an orthotopic *in vivo* xenograft model. Growth reduction after rigosertib treatment was observed in 3/8 HNSCC direct patient tumor lines. The responsive tumor lines carried a combination of a *PI3KCA* activating event (amplification or mutation) and a p53 inactivating event (either HPV16-mediated or mutation-mediated *TP53* inactivation). In this study, we evaluated the *in vitro* and *in vivo* efficacy of rigosertib in both HPV+ and HPV− HNSCCs focusing on inhibition of the PI3K pathway. Although consistent inhibition of the PI3K pathway was not evident in HNSCC, we identified a combination of *PI3K*/*TP53* events necessary, but not sufficient for rigosertib-sensitivity.

Keywords

Head and neck squamous cell cancer; Human papilloma virus; Rigosertib; PI3K; TP53

Corresponding Author: Antonio Jimeno M.D., Ph.D., Associate Professor of Medicine/Oncology and Otolaryngology, University of Colorado School of Medicine, 12801 East 17th Avenue, Room L18-8101B, Aurora, CO 80045, Antonio.Jimeno@ucdenver.edu.
*Denotes equal contribution

Conflict of Interest: The authors declare no conflict of interest.

INTRODUCTION

Squamous cell carcinoma of the head and neck (HNSCC) is the sixth-most frequent cancer worldwide by incidence. Originating in the mucosa of the upper airways, one-third of patients present with early-stage disease while the majority present with advanced disease and lymph node metastasis (1). Current estimates suggest that over 600,000 cases will arise globally in 2012 with a 5 year patient survival rate of 40–50% (2), that has not improved substantially despite advances in anticancer therapy. Tobacco and alcohol consumption have historically been the most important risk factors, and incidence of HNSCC in the western world had been on a slow decline over the past decade correlated with decline in tobacco use (3). However, a subgroup of HNSCCs associated with high-risk human papillomavirus (HPV) infection, notably in the oropharynx, is becoming more prevalent (4).

Meta-analysis data suggests that HPV is detectable in 26–35% of HNSCC patients (5). Data from the Surveillance, Epidemiology, and End Results (SEER) Program documented an increase in HPV-serotype16 (HPV16) oropharyngeal squamous cell carcinomas from 16% to 72%, particularly in young (<60 years of age) Caucasian males between 1984 and 2004 (6).

High-risk HPV infection leads to genetic instability by impairing the tumor suppressors TP53 and Rb via the E6 and E7 viral oncoproteins, respectively (7). Due to their distinct molecular driver, the progression of HPV+ HNSCCs is different from cancers associated with alcohol and tobacco use (8). The rate of mutation in HPV+ tumors was half the rate observed in HPV− tumors (9). While HPV+ HNSCC has a more favorable prognosis than HPV− (10), it can be hypothesized that this dramatically different pathogenesis will require alternative therapeutic approaches. Expression of the HPV16 oncoprotein E7 upregulates Akt activity in human keratinocytes, which is likely a contributing factor to transformation (11, 12), and E7 enhances keratinocyte migration in a PI3K/Akt-dependent manner (13). There is evidence that E6, in addition to labeling p53 for degredation, differentially modulates the PI3K signaling pathway (14), and that E6-driven activation of PI3K/Akt confers resistance to cisplatin in HPV+ cancers (15). Furthermore, HPV+ cases have a higher rate of activating canonical phosphoinositide-3-kinase catalytic α (*PIK3CA*) mutations (9, 16). The link between PI3K/Akt activation and HPV infection suggests that PI3K inhibition may be an appropriate therapeutic approach for HPV+ HNSCC.

PIK3CA copy number changes have also been documented in HPV− tumors, making *PIK3CA* relevant in both HPV+ and HPV− HNSCC subtypes (17). PI3K transduces stimuli involved in the regulation of several processes involved in transformation including neovascularization, proliferation, cell motility, adhesion, survival and apoptosis (18, 19). A direct association between enhanced PI3K/Akt pathway activation and tumor formation within HNSCC has been identified (17, 20, 21), and dysregulation and/or genetic aberrations of the *PI3KCA*, *Akt*, and phosphatase and tensin homologue (*PTEN)* have been associated with HNSCC development (22). Targeted therapeutic agents to members of this pathway are currently being evaluated in several cancer types (23).

Direct binding of p53 to the promoter induces transcriptional inhibition of *PIK3CA* (24). *TP53* is the most commonly altered gene in HPV− HNSCCs, with mutations found in 78% of patients not infected by a high-risk HPV subtype (16). It has been well established that mutations within the DNA binding domain result in a loss of function phenotype and correlate with a more advanced tumor stage at diagnosis, a high incidence of lymph node metastasis, and may predict suboptimal patient response to traditional therapeutic treatment regimens (25–27). *TP53* status is an important diagnostic consideration, especially in HPV−

HNSCCs. Patients infected with HPV have non-functioning p53 due to E6-driven destruction (7).

Rigosertib (ON 01910.Na, Estybon) is a non-ATP competitive small molecule targeted agent that inhibits PI3K/Akt pathway activation and disrupts PLK1-mediated G_2-M transition (28, 29). Although it was initially thought that direct inhibition of PLK1 was responsible for the observed antimitotic activity, subsequent studies did not support a direct effect on polo-like kinases (30). Direct inhibition of PI3K has been observed in mantle cell lymphoma (MCL) cell lines treated with rigosertib (31). Inhibition of PI3K signaling was later confirmed in chronic lymphocytic leukemia cells (28). This agent is unique in its ability to impair both cell signaling and mitosis. Rigosertib is currently being evaluated in Phase II clinical trials as a single agent for squamous cell carcinomas and hematologic malignancies, and with gemcitabine for pancreatic cancer.

In this study, we aimed to evaluate the efficacy of PI3K inhibition by rigosertib in HNSCC both *in vitro* and *in vivo*. Furthermore, we investigated the differential response to treatment in correlation to HPV status, genetic aberrations, and signaling pathway modulation in an effort to identify biological markers predictive of treatment outcome.

MATERIAL AND METHODS

Cell lines and *in vitro* drugs

HNSCC cell lines were commercially acquired and/or obtained from David Sidransky (Johns Hopkins University) and Barbara Frederick (University of Colorado); cell lines were grown in DMEM supplemented with 10% FBS, 200 μg/mL penicillin, and 200 μg/mL streptomycin. Low serum media (LSM) contained 0.5% FBS. Cell lines were authenticated after receipt by mitochondrial DNA sequencing, and passaged for less than 6 months following authentication. Mycoplasma was tested for using the MycoAlert Mycoplasma assay (Lonza). All cultures tested negative. ZSTK474 was acquired commercially. The chemical structure of rigosertib has been published previously (32), and the drug was supplied by Onconova Therapeutics, Inc.

In vitro colony formation assay

Cells were seeded 300 cells/well in 6-well plates and incubated for 24 hrs. Media containing either vehicle or 1.0 μM drug was added and plates were incubated for 7 days. Resulting colonies (>50 cells) were fixed with 4% formalin and stained using 0.1% crystal violet.

Sulforhodamine B Colorimetric assay (SRB)

Cells (2,500–5,000) were plated in 96-well plates and incubated overnight. Drug was added and plates were incubated for 96 hrs. Cells were fixed with 50 μl of 10% TCA at 4°C (30 min) and washed 5X with dH_20. Next 70 μl/well SRB reagent was added, wells were washed 5X with 1% acetic acid, 200 μl/well 10 mMTris base was added, plates were shaken at 40 rpm at RT (15 min), and absorbance was measured using a Synergy 2 microplate reader (Bio-Tek).

Cell cycle analysis by flow cytometry

Cells (1×10^6) were trypsinized, centrifuged, and resuspended in cold PBS then fixed by adding cold 100% ethanol drop-wise until reaching a final concentration of 70% then incubating for 20 mins at 4°C. The cells were suspended propridium iodide buffer (50 μg/ml) in PBS and incubated for 1 hr at room temperature. Samples were analyzed on a Cyan flow cytometer (Beckman Coulter).

Microarray Analysis

Total RNA was isolated using the RNeasy Mini Kit (Qiagen) according to the manufacturer's instructions. Samples were analyzed on the Human Gene 1.0 Array (Affymetrix). Arrays were normalized with the robust multichip average (RMA) algorithm, and probe sets were collapsed to genes by finding the maximum signal for each gene (33). Gene set enrichment analysis (GSEA, v. 2.07) was conducted on the collapsed data using the Kyoto Encyclopedia of Genes and Genomes (KEGG) and Biocarta pathway definitions obtained from the Molecular Signatures Database v. 3.1 (34). All analyses except GSEA were conducted in R/Bioconductor v. 2.11. Relevant pathways with a nominal p-value ≤0.1 for the KEGG and ≤0.05 for the Biocarta databases were included in the analysis. The microarray data sets were uploaded to the GEO repository (accession number: GSE47864).

Human xenograft generation and *in vivo* studies

Fresh tumor tissue was collected, from HNSCC patients consented at the University of Colorado Hospital in accordance with the protocol approved by the Colorado Multiple Institutional Review Board (COMIRB # 08-0552). Tissue was prepared from 3×3×3 mm tumor pieces dipped in Matrigel (BD Biosciences) and inserted subcutaneously into both hind flanks of nude mice. Upon reaching 1500 mm3, tumors were passed to a second colony of animals for therapeutic studies.

Eight patient cases were treated with rigosertib. For each case, we implanted 20 tumors in 10 mice. When tumors reached 200 mm^3 mice were distributed into 2 groups (at least n=8 tumors per group) and treated: control or rigosertib, 250 mg/kg administered 5X/week IP for 4 weeks. Tumor size was evaluated twice weekly using the formula: volume = [length × $width^2$]/2. Six hours after the last drug administration, tumors were extracted and portions were flash-frozen and embedded in paraffin.

Cancer cell lines were injected orthotopically in the floor of the mouth of athymic nude mice at a concentration of 10^6 cells/50 μL suspended in 50:50 DMEM to Matrigel (BD Biosciences). Once tumor volumes reached an average of 100 mm^3, mice were randomly distributed into 2 groups (at least n=7 tumors per group) and evaluated as previously described.

Fluorescence in situ hybridization (FISH)

Slides were incubated at 56°C for 4 hrs, soaked in CitriSolv 3 times for 5 min each, dehydrated and allowed to air dry. The tissue area to be hybridized was marked with a diamond pen. The slides were incubated in pretreatment solution at 80°C for ~12min, in protease solution IV at 37°C for ~20 min, washed in milli-Q water at room temperature, dehydrated and air dried. The 3-color probe mixture was applied to the selected hybridization areas, covered with coverslips and sealed with rubber cement. DNA codenaturation was performed at 76°C for 5 min in a thermocycler and hybridization was allowed to occur at 37°C for 40–48 hours. Post-hybridization washes were performed through incubations in 2xSSC/0.3% NP-40 at 74°C for 2 min and 2xSSC for 2 min each, followed by dehydration. Finally, 14 μl of DAPI/anti-fade (0.3 μg/ml in Vectashield mounting medium) was applied to the slide and the area covered with a 22×50 mm coverslip. Analysis was performed on epifluorescence microscopes using single interference filters sets for green (FITC), red (Texas red), blue (DAPI), gold, dual (red/green), and triple (blue, red, green) band pass filters. For each interference filter, monochromatic images were acquired and merged using CytoVision (Leica Microsystems Inc.).

Human papillomavirus detection

In situ hybridization for HPV low and high-risk types was conducted using the Ventana INFORM HPV III automated assays (Ventana Medical Systems) on 4 μm paraffin embedded tissue sections. The Benchmark system uses the Ventana ISH-Protease 3 enzyme to remove proteins surrounding the target DNA. A biotinylated antiflourescin antibody is used to detect the hybridized probe, followed by streptavidin to bind biotin and then a chromagen reaction with nitoblue tetrazolium and 5-Bromo-4-chloro-3-indolyl-phosphate for detection.

Immunohistochemistry (IHC)

For IHC staining, slides were de-paraffinized and re-hydrated in graded concentrations of alcohol by standard techniques before antigen retrieval in citrate buffer pH 6.0 (Dako Corperation) at 105°C for 20 min. Next, slides were cooled for 20 min before washing. All staining was done in a Dako Autostainer. Slides were incubated in 3% H_2O_2 for 10 min, followed by primary 2211 pS6K, 3787 pAkt, 9559 PTEN or 4376 pMAPK, (Cell Signaling Technologies) and incubated for 60 min at RT. Staining was developed by: EnVision+ Dual Link System HRP (Dako) for 30 min and substrate-chromogen (DAB+) Solution (Dako) for 7 min. Slides were then counterstained with Automated Hematoxylin (Dako) for 5 min. The intensity (0,1+,2+,3+) and the percentage (0–100%) of cells positive were interpreted blinded and in triplicate to the case and treatment. Reported IHC scores were calculated by multiplying the population % by the intensity (0, 1, 2, 3) then averaging the values for the triplicate reads for each sample.

DNA Sequencing

PCR amplification reactions were carried out in 96-well ABI Veriti thermocycler (Applied Biosystems) using a touchdown PCR protocol as described (35). DNA sample quality and concentrations were assessed by gel electrophoresis. PCR amplification and Sanger sequencing were performed using primer sets referenced in Agrawal et al. [16]. PCR product was directly sequenced using the BigDye Terminator Cycle Sequencing Ready Reaction kit version 1.1 (Applied Biosystems). The standard sequencing thermo-cycling parameters were as follows: denaturation for 5 min at 94°C, followed by 30 cycles of denaturation at 96°C for 10 sec, annealing at 50°C for 5 sec, and extension/termination at 60°C for 4 min, followed by incubation at 10°C until the samples were processed. Residual dye-labeled dideoxynucleotides (dye-terminators) were removed from the cycle-sequencing reaction products using the paramagnetic bead technology CleanSEQ from Agencourt Bioscience Corporation or PureSeq from Aline Biosciences, and a modification of the manufacturers' recommended protocol. The products were sequenced on a fluorescent capillary automated sequencer - an Applied Biosystems/Hitachi 3730 Genetic Analyzer with a 50 cm long, 48-capillary array containing POP7 polymer. Analyses of DNA sequences were done with Sequencing Analysis version 5.2 and Sequence Scanner version 1.0 (both from Applied Biosystems). Alignments of DNA sequences were done with Sequencher 4.8 (Gene Codes Corporation) and/or SeqScape (Applied Biosystems). PCR product sequence comparison to GenBank reference sequence and mutation identification were accomplished using Mutation Surveyor version 4.0.4 (SoftGenetics).

SNaPshot Assay

The Colorado Molecular Correlates (CMOCO) SNaPshot panel tests for 68 discrete mutational loci, 8 of which are validated for treatment guidance in non-small cell lung carcinoma. Briefly, after nucleic acid is extracted, target regions of the 15 tested genes are PCR amplified with multiplex primer sets. After phophatase and exonuclease treatment to remove unincorporated dNTS and primers, the PCR products are then used as a template for

labeled single base extension using matched probe sets. The resulting SNaPshot products are analyzed with capillary electrophoresis and resultant data analyzed for the presence of mutations. Determination of the presence or absence of mutation is carried out by manual evaluation of the data examined through Genemapper software.

Western blotting

Cell pellets were lysed in 30–100 μl RIPA lysis buffer containing 5 μl/ml PMSF. Tissue sample (50 mg) portions were thawed in a 4X volume of RIPA Buffer and homogenized using single-use plastic pestles. Protein was measured using the ELx800 absorbance microplate reader (BioTek) according to the manufacturer's instructions. 30 ng of protein was loaded per well into NuPage Novex 4–12% Bis-Tris Midi Gel (Invitrogen), transferred using the iBlot Gel Transfer Stack System (Invitrogen) then processed. Primary antibodies were purchased from Cell Signaling Technologies: 4060 pAkt, 4821 Akt, 4094 pMAPK, 9102 MAPK, 2215 pS6RP, 2217 S6RP, and 4968 Pan-Actin. Antibody specificity as determined by an isotype control was completed by the manufacturer. Secondary anti-rabbit IgG (Immuno Research) was used at a 1:50,000 dilution. The signal was visualized using Immuobilon Western chemiluminescent HRP substrate (Millipore).

RESULTS

Rigosertib induces a potent antiproliferative effect in HNSCC cell lines

We investigated rigosertib activity in a panel of 16 immortalized HNSCC cell lines. Eleven of 16 cell lines showed potent antiproliferative activity at sub-μM concentrations (Fig. 1A). Three cell lines had a moderate response to treatment, and proliferation of 2 cell lines (MSK921 and UMSCC19) was unaffected at concentrations up to 10 μM. All HNSCC cell lines tested HPV−.

We chose 2 sensitive (584 and HN11) and 2 resistant (MSK921 and UMSCC19) cell lines for further investigation of changes in gene expression and PI3K pathway activation. Treatment sensitivity for these cell lines was confirmed by clonogenic assay (Fig. 1B). Sensitivity to treatment at 1.0 μM was comparable to the SRB assay results.

Differential gene set enrichment in the rigosertib sensitive vs. resistant cell lines

We then sought to correlate global gene expression to rigosertib sensitivity (≤15% or ≥45% proliferation after 1.0 μM rigosertib treatment, respectively) using the Affymetrix microarray platform. Gene set enrichment analysis (GSEA) was used to identify pathways enriched in the rigosertib sensitive and resistant cohorts. Several cancer-related KEGG gene sets were enriched in the more resistant cohort. KEGG gene sets enhanced in resistant cell lines with a false discovery rate (FDR q-val) <25% included pancreatic cancer and DNA replication (Table 1). Biocarta pathways involved in endocytosis were also enriched. This is particularly interesting because of the overlap between differential phosphorylation patterns of phosphoinositides (PIs) in both the regulation of endocytic trafficking and their involvement in the PI3K signal transduction pathway (36).

The hedgehog, MAPK, calcium, and gap junction signaling pathway gene sets, all of which include members of key pathways associated with HNSCC development, progression and maintenance, were enriched in the sensitive cell lines in the KEGG data set (Supplementary Table 1) (4). Interestingly, the two pathways enriched in the Biocarta dataset involve anti-apoptotic pathway activation through the PI3K/Akt, MAPK and Src pathways. We then extracted core genes for PI3K related pathways within the top 50 pathways identified by GSEA for both data sets. Employing heat maps, we compared sensitive and resistant cell

lines revealing enrichment in this gene set in the sensitive cell lines (Supplementary Fig. 1C).

Antiproliferative effects of rigosertib result from an inhibition of more than one pathway in HNSCC cell lines

We then investigated the mutation status of our chosen four cell lines by full exon sequencing of *PIK3CA* and *TP53,* and by the multiplexed-PCR based SNaPshot assay; a technology capable of simultaneously identifying mutational status at 68 hot spot loci (37). Poly Phen-2 analysis was used to interpret the effect of identified amino acid substitutions (38). The resistant cell line UMSCC19 harbored a H1047R activating mutation in *PIK3CA* exon 20 (Table 2). This mutation has been cited as oncogenic in ovarian and breast cancers (39). Two heterozygous mutations were documented in the DNA binding region of *TP53* in the resistant cell line MSK921, both predicted as damaging by Poly Phen-2 analysis. These mutations likely impair DNA binding by p53. Broad genotyping by SNaPshot confirmed the H1047R substitution in UMSCC19, but identified no other mutations. Both the sensitive cell lines were *TP53* and *PIK3CA* wild type. *PIK3CA* activating mutations did not correlate with a rigosertib treatment sensitive phenotype.

We extended our full exon sequencing and SNaPshot platforms to characterize the mutational status of the full panel of HNSCC cell lines (Supplementary Table 2). Eight of 16 cell lines harbored inactivating mutations in *TP53*. There was no noticeable trend between *TP53* mutation status and treatment sensitivity. Interestingly, Detroit 562 harbored a mutation in both genes, and was sensitive to treatment with rigosertib.

Phosphorylation patterns of Akt and S6 following rigosertib treatment were not uniformly observed across our panel of HNSCC cell lines (Fig. 1C). The phosphorylation of Akt at Ser473 in HN11 and MSK921 was reduced with treatment, and a corresponding reduction of S6 phosphorylation was observed. However, there was no decrease in phosphorylation in 584 or UMSCC19. Conversely, there was complete inhibition of Akt and S6 phosphorylation following treatment with ZSTK474, which binds directly to the PI3K ATP binding site, in all four cell lines. Furthermore, the antiproliferative profile of ZSTK474 in these cell lines was very different than that of rigosertib (Supplementary Fig. 2). Next, we stained for MAPK signaling pathway modulation that was relatively inconsistent (Supplementary Fig. 3).

We then examined cell cycle progression of treated cells by flow cytometry (Fig. 1D). Whereas treatment with rigosertib generated a complete G2 block in both sensitive cell lines and a partial build-up of G2 phase in the resistant lines, cells treated with a specific PI3K inhibitor ZSTK474 arrested all four cell lines, sensitive and resistant to rigosertib, in G1 phase at 24 hours post treatment. This data suggests that PI3K inhibition alone does not explain the antiproliferative effects of rigosertib; instead, the antimitotic and G2/M arresting effects likely play a key role.

Rigosertib sensitivity confirmed in HNSCC cell lines implanted orthotopically in athymic nude mice

We confirmed rigosertib activity in the sensitive HNSCC cell lines using an orthotopic xenograft platform. Cell lines were injected into the floor of the mouth of the mice to better replicate the tumors origin microenvironment (Fig. 2A). After 28 days of treatment, tumor regression and growth reduction were observed in rigosertib treated 584 and HN11 implanted mice, respectively, compared to the untreated control group. We used fluorescence *in situ* hybridization (FISH) to identify if there was gene copy number gain for *PIK3CA* in these tumors (Fig. 2B and Supplementary Table 3). 584 showed no copy number

gain with a representative FISH score of 2. HN11 showed a low copy number gain with a representative FISH score of 3. Western blot analysis of treated tissue did not confer PI3K/Akt pathway inhibition in the xenografted cell lines (Fig. 2C). These observations were confirmed by IHC (Fig. 2D and Supplementary Fig. 4A). This contrasts with the observed Akt and S6 phosphorylation patterns in HN11, although modest, *in vitro*. Our results confirm rigosertib sensitivity profiles in these cell lines in a xenograft model, and further suggest that rigosertib's antiproliferative properties do not result solely from an inhibition of the PI3K pathway. Previous reports have documented G2/M arrest and alteration in the mitotic pathway and centrosomal changes as key parts of anticancer effect of rigosertib (40). Thus multiple pathway inhibition is involved in the antiproliferative and biochemical effects of rigosertib.

Rigosertib is active in direct patient xenografted tumor lines

We treated 8 cohorts of HNSCC direct-patient tumor xenografts implanted in immunocompromised mice with rigosertib. Half of the chosen tumor lines were positive for HPV16 infection: CUHN014, CUHN022, CUHN043 and CUHN047. Tumor measurements normalized to the average volume of the control group taken on day 28 from each study are shown in Fig. 3A and Supplementary Fig. 5. Growth reduction >50%with rigosertib therapy was observed in CUHN014, CUHN047 and CUHN026. No significant response was observed in the remaining 5 tumor lines. The two lines most sensitive to treatment, CUHN014 and CUHN047, both were HPV+. However, two resistant lines, CUHN043 and CUHN022, were also HPV+.

We explored whether amplification of *PIK3CA* may yield a more sensitive phenotype to rigosertib treatment. A high prevalence of gene copy number gain abnormalities exists in HNSCC (17). Three of the eight tumor lines scored positive for *PIK3CA* gene amplification; a representative FISH score of 5 (Fig. 3B and Supplementary Table 4). Two of them, CUHN014 and CUHN047, were sensitive to treatment with rigosertib. The resistant tumor lines CUHN025, CUHN043, and CUHN022 all had either no or low copy gain. High copy number gain was identified in CUHN026 and CUHN040.

Western blot analysis of PI3K pathway components yielded inconsistent results (Fig. 3C and Supplementary Fig. 6). There was no emerging trend observed after staining for phosphorylated Akt or its negative regulator PTEN (Fig. 3D). Reduction in phosphorylation levels of S6 ribosomal protein were observed in the western blot staining for CUHN047 and CUHN026 while CUHN014 did not have a significant change when compared with total S6 staining. Reduction of phosphorylation of S6 ribosomal protein was observed in all three sensitive lines by IHC, although not to a significant level in CUHN014. Reduced phosphorylation was also observed in the resistant line CUHN013. The western blot trends observed for the other members of these pathways were confirmed by IHC (Fig. 3D and Supplementary Fig. 7).

A combination of PIK3CA and TP53 genetic events correlate with a rigosertib sensitive phenotype

Exon sequencing of *PIK3CA* and *TP53* was completed for the treated with rigosertib (Table 3). A heterozygous E545K substitution in *PI3KCA* was identified in CUHN026 xenograft. This variant has been catalogued as an activating mutation located within the helical domain (41). Growth of CUHN026 was reduced with rigosertib treatment, consistent with our hypothesis that rigosertib treatment will have a more potent effect in the presence of PI3K pathway activation. *TP53* somatic mutations were identified in 3 tumor lines. These mutations are located within the DNA binding domain, which suggests they are inactivating. Analysis using the PolyPhen-2 program scored all mutations as probably damaging.

Interestingly, the responsive tumors lines all have a *PIK3CA* genetic event, be it amplification or activating mutation, and are either HPV16-positive or harbor an inactivating *TP53* mutation. CUHN013 was not susceptible to rigosertib despite harboring *PI3KCA* amplification and *TP53* mutation. However, CUHN013 is highly EGFR dependent (42), which may explain resistance to a targeting agent that does not directly inhibit EGFR pathway activation. Additionally, factors other than these two may influence susceptibility to rigosertib. While the PI3K pathway may not be the primary target of rigosertib in HNSCC, our data suggests that the combination of a *PIK3CA* activating event with a *TP53* inactivating event is necessary, but not sufficient, for sensitivity to rigosertib treatment in HNSCC xenografts.

DISCUSSION

Dysregulation of the PI3K pathway in HNSCCs is frequent, and contributes to amplified growth advantage, increased metastatic potential and resistance to therapeutic regimen. In accordance with published data, our lab has identified genomic alterations of PI3K occurring in 20% of our tumor lines generally, and in 40% of HPV-positive tumors (16, 43). Furthermore, several studies have evaluated the predictive correlation of common PI3K aberrations and drug specific treatment outcome (44–46). The established importance of PI3K, as not only a therapeutic target but also a predictive biomarker, confers the relevance of a multifaceted focus on this pathway in the field of head and neck oncology.

Inhibition of the PI3K/Akt signaling pathway in MCL cell lines and chronic leukemia cell lines, preliminary treatment response data in solid tumors, and clinical relevance supports evaluating rigosertib as a treatment for HNSCC (31, 47, 48). We observed potent antiproliferative activity by rigosertib in our panel of HNSCC cell lines. Only 2 cell lines were resistant to treatment with an IC_{50}>10.0 μM. Rigosertib completely inhibited colony formation at 10.0 μM in both sensitive and resistant cell lines. There was no correlation with treatment response in our panel of 17 HNSCC cell lines and mutation profile of either *TP53* or *PIK3CA* alone. However, consistent with the predictive biomarker combination we identified in our tumor lines, rigosertib-sensitive Detroit 562 harbored an inactivating *TP53* mutation in combination with an activating *PIK3CA* mutation.

Treatment sensitivity of HN11 and 584 was confirmed by *in vivo* treatment studies when orthotopically xenografted. Regression and significant growth reduction were observed in 584 and HN11 engrafted tumors respectively. Rigosertib treatment also induced growth reduction in 3/8 HNSCC patient tumor lines. Efficacy both *in vitro* and *in vivo* substantiates rigosertib as a promising targeted agent for clinical evaluation in HNSCC.

Several PI3K-related gene sets were enriched in the pathways identified by GSEA in the KEGG and Biocarta databases derived from *in vitro* microarray results. However, PI3K pathway modulation was inconsistent for HNSCCs both *in vitro* and *in vivo*. No general inhibitory trend was observed for the phosphorylation of Akt at serine residue 473, or of S6 ribosomal protein at serine residues 240/244, events indicative of PI3K pathway activation. Cell cycle analysis of HNSCC cell lines treated with rigosertib yielded results more representative of those expected from a cytotoxic drug, a complete G2 block in sensitive lines, than to those obtained with the PI3K targeting agent ZSTK474 (49). These studies confirm earlier observations indicating that multiple mechanisms are involved in the activity of rigosertib, including effects on signal transduction and mitotic pathways. Such complexity of action likely explains the breadth of activity observed *in vitro*. Depending on the cell-type and genetic background inhibition of one pathway may dominate over another.

Merit to the relationship between rigosertib treatment and the PI3K pathway is conferred by the prognostic value of PI3K aberrations. Interactions betweenTP53 and the PI3K/Akt pathway have been shown to play a significant role in apoptosis and cell survival (50). It has further been documented that amplified PI3K pathway activation correlates with HPV-positivity in HNSCCs due to the loss of attenuation at the *PIK3CA* promoter (51). Here, we have observed a correlation between rigosertib sensitivity and the co-existence of both a *PIK3CA* activating event, be it mutation or amplification, and either a deleterious *TP53* mutation or p53 inactivation by HPV16 infection. For example, UMSCC19 harbors a *PIK3CA* mutation but lacks *TP53* inactivation, and is resistant to rigosertib. However, CUHN013 has *PIK3CA* amplification and is a *TP53* mutant but is rigosertib-resistant. Decreased phosphorylation of S6 after treatment with rigosertib was also observed, suggesting that the PI3K pathway is inhibited in this tumor line. However, xenograft treatment studies using the EGFR targeting agent cetuximab induced remission in a 28-day animal treatment study in CUHN013 (42). This is evidence of EGFR-dependence, and provides a possible mechanism of resistance to rigosertib treatment.

Our data suggests that the combination of a *PIK3CA* activating event and p53 inactivating event is necessary, but not sufficient, for a rigosertib-sensitive phenotype. Similarly, cooperation between $PIK3CA^{H1047R}$ and p53 loss-of-function mutations was identified in mouse mammary tumor formation (52). The double-mutant mice formed a spectrum of tumors unique from those of the $PIK3CA^{H1047R}$ single-mutant strain. This indicates that the combination of these events results in a distinct mechanism of PI3K pathway activation, which may explain differential rigosertib treatment response.

A phase 1 study of oral rigosertib treatment in patients with advanced solid tumors recently concluded at the University of Colorado School of Medicine, and rigosertib showed efficacy in 2/8 HNSCC patients treated (53). One of the responsive patients harbored an inactivating *TP53* mutation in combination with *PIK3CA* gene amplification. The second responder was HPV+ and harbored a *PTEN* loss, highlighting the presence of abnormalities in TP53 function and PI3K/Akt pathway in susceptible cases. The rate of response in HNSCC patients was very similar in this subset with 8 HNSCC subjects and in the HNSCC xenograft set of 8 cases. However given the relatively small number of HNSCC cases presented here and the small number of patients in the Phase 1 study, this data is hypothesis-generating. A multicenter phase 2 study of oral rigosertib treatment in relapsed or metastatic SCC is underway, includes comprehensive genomic testing (SNaPShot and DNAseq in all patients), and will have the statistical power to fully examine this hypothesis.

Supplementary Material

Refer to Web version on PubMed Central for supplementary material.

Acknowledgments

Grant Support

This work was supported by National Institutes of Health R21 DE019712, R01 CA149456, and the Cancer Center Support Grant P30 CA046934 (issued to A. Jimeno). Additionally supported by Onconova Therapeutics, Inc. (issued to A. Jimeno).

Bibliography

1. Haddad RI, Shin DM. Recent advances in head and neck cancer. New Engl J Med. 2008; 359:1143–54. [PubMed: 18784104]

2. Wilken R, Veena MS, Wang MB, Srivatsan ES. Curcumin: A review of anti-cancer properties and therapeutic activity in head and neck squamous cell carcinoma. Molecular cancer. 2011; 10:12. [PubMed: 21299897]

3. Cardesa A, Nadal A. Carcinoma of the head and neck in the HPV era. Acta Dermatovenerol Alp Panonica Adriat. 2011; 20:161–73. [PubMed: 22131117]

4. Leemans CR, Braakhuis BJ, Brakenhoff RH. The molecular biology of head and neck cancer. Nat Rev Cancer. 2011; 11:9–22. [PubMed: 21160525]

5. Kreimer AR, Clifford GM, Boyle P, Franceschi S. Human papillomavirus types in head and neck squamous cell carcinomas worldwide: a systematic review. Cancer Epidemiol Biomarkers Prev. 2005; 14:467–75. [PubMed: 15734974]

6. Chaturvedi AK, Engels EA, Pfeiffer RM, Hernandez BY, Xiao W, Kim E, et al. Human papillomavirus and rising oropharyngeal cancer incidence in the United States. J Clin Oncol. 2011; 29:4294–301. [PubMed: 21969503]

7. Duensing S, Munger K. Mechanisms of genomic instability in human cancer: insights from studies with human papillomavirus oncoproteins. International Journal of Cancer. 2004; 109:157–62.

8. Myers EN. Head and neck oncology--2010, Part I. Otolaryngol Pol. 2010; 64:136–46. [PubMed: 20731202]

9. Stransky N, Egloff AM, Tward AD, Kostic AD, Cibulskis K, Sivachenko A, et al. The mutational landscape of head and neck squamous cell carcinoma. Science. 2011; 333:1157–60. [PubMed: 21798893]

10. Weinberger PM, Yu Z, Haffty BG, Kowalski D, Harigopal M, Brandsma J, et al. Molecular classification identifies a subset of human papillomavirus--associated oropharyngeal cancers with favorable prognosis. J Clin Oncol. 2006; 24:736–47. [PubMed: 16401683]

11. Pim D, Massimi P, Dilworth SM, Banks L. Activation of the protein kinase B pathway by the HPV-16 E7 oncoprotein occurs through a mechanism involving interaction with PP2A. Oncogene. 2005; 24:7830–8. [PubMed: 16044149]

12. Menges CW, Baglia LA, Lapoint R, McCance DJ. Human papillomavirus type 16 E7 up-regulates AKT activity through the retinoblastoma protein. Cancer research. 2006; 66:5555–9. [PubMed: 16740689]

13. Charette ST, McCance DJ. The E7 protein from human papillomavirus type 16 enhances keratinocyte migration in an Akt-dependent manner. Oncogene. 2007; 26:7386–90. [PubMed: 17533372]

14. Contreras-Paredes A, De la Cruz-Hernandez E, Martinez-Ramirez I, Duenas-Gonzalez A, Lizano M. E6 variants of human papillomavirus 18 differentially modulate the protein kinase B/phosphatidylinositol 3-kinase (akt/PI3K) signaling pathway. Virology. 2009; 383:78–85. [PubMed: 19007961]

15. Wu HH, Wu JY, Cheng YW, Chen CY, Lee MC, Goan YG, et al. cIAP2 upregulated by E6 oncoprotein via epidermal growth factor receptor/phosphatidylinositol 3-kinase/AKT pathway confers resistance to cisplatin in human papillomavirus 16/18-infected lung cancer. Clin Cancer Res. 2010; 16:5200–10. [PubMed: 20959404]

16. Agrawal N, Frederick MJ, Pickering CR, Bettegowda C, Chang K, Li RJ, et al. Exome Sequencing of Head and Neck Squamous Cell Carcinoma Reveals Inactivating Mutations in NOTCH1. Science. 2011; 333:1154–7. [PubMed: 21798897]

17. Woenckhaus J, Steger K, Werner E, Fenic I, Gamerdinger U, Dreyer T, et al. Genomic gain of PIK3CA and increased expression of p110alpha are associated with progression of dysplasia into invasive squamous cell carcinoma. The Journal of pathology. 2002; 198:335–42. [PubMed: 12375266]

18. Datta SR, Brunet A, Greenberg ME. Cellular survival: a play in three Akts. Genes & development. 1999; 13:2905–27. [PubMed: 10579998]

19. Nicholson KM, Anderson NG. The protein kinase B/Akt signalling pathway in human malignancy. Cellular Signalling. 2002; 14:381–95. [PubMed: 11882383]

20. Estilo CL, POC, Ngai I, Patel SG, Reddy PG, Dao S, et al. The role of novel oncogenes squamous cell carcinoma-related oncogene and phosphatidylinositol 3-kinase p110alpha in squamous cell

carcinoma of the oral tongue. Clinical cancer research: an official journal of the American Association for Cancer Research. 2003; 9:2300–6. [PubMed: 12796399]

21. Or YY, Hui AB, Tam KY, Huang DP, Lo KW. Characterization of chromosome 3q and 12q amplicons in nasopharyngeal carcinoma cell lines. International journal of oncology. 2005; 26:49–56. [PubMed: 15586224]
22. Bunney TD, Katan M. Phosphoinositide signalling in cancer: beyond PI3K and PTEN. Nat Rev Cancer. 2010; 10:342–52. [PubMed: 20414202]
23. Howard JD, Lu B, Chung CH. Therapeutic targets in head and neck squamous cell carcinoma: identification, evaluation, and clinical translation. Oral Oncol. 2012; 48:10–7. [PubMed: 22020057]
24. Astanehe A, Arenillas D, Wasserman WW, Leung PC, Dunn SE, Davies BR, et al. Mechanisms underlying p53 regulation of PIK3CA transcription in ovarian surface epithelium and in ovarian cancer. Journal of cell science. 2008; 121:664–74. [PubMed: 18270270]
25. Erber R, Conradt C, Homann N, Enders C, Finckh M, Dietz A, et al. TP53 DNA contact mutations are selectively associated with allelic loss and have a strong clinical impact in head and neck cancer. Oncogene. 1998; 16:1671–9. [PubMed: 9582015]
26. Perrone F, Bossi P, Cortelazzi B, Locati L, Quattrone P, Pierotti MA, et al. TP53 Mutations and Pathologic Complete Response to Neoadjuvant Cisplatin and Fluorouracil Chemotherapy in Resected Oral Cavity Squamous Cell Carcinoma. J Clin Oncol. 2010; 28:761–6. [PubMed: 20048189]
27. Skinner HD, Sandulache VC, Ow TJ, Meyn RE, Yordy JS, Beadle BM, et al. TP53 Disruptive Mutations Lead to Head and Neck Cancer Treatment Failure through Inhibition of Radiation-Induced Senescence. Clinical Cancer Research. 2012; 18:290–300. [PubMed: 22090360]
28. Chapman CM, Sun X, Roschewski M, Aue G, Farooqui M, Stennett L, et al. ON 01910.Na is selectively cytotoxic for chronic lymphocytic leukemia cells through a dual mechanism of action involving PI3K/AKT inhibition and induction of oxidative stress. Clinical cancer research: an official journal of the American Association for Cancer Research. 2012; 18:1979–91. [PubMed: 22351695]
29. Gumireddy K, Reddy MV, Cosenza SC, Boominathan R, Baker SJ, Papathi N, et al. ON01910, a non-ATP-competitive small molecule inhibitor of Plk1, is a potent anticancer agent. Cancer Cell. 2005; 7:275–86. [PubMed: 15766665]
30. Lenart P, Petronczki M, Steegmaier M, Di Fiore B, Lipp JJ, Hoffmann M, et al. The small-molecule inhibitor BI 2536 reveals novel insights into mitotic roles of polo-like kinase 1. Curr Biol. 2007; 17:304–15. [PubMed: 17291761]
31. Prasad A, Park IW, Allen H, Zhang X, Reddy MV, Boominathan R, et al. Styryl sulfonyl compounds inhibit translation of cyclin D1 in mantle cell lymphoma cells. Oncogene. 2009; 28:1518–28. [PubMed: 19198627]
32. Nuthalapati S, Zhou Q, Guo P, Lv H, Cosenza S, Reddy MV, et al. Preclinical Pharmacokinetic and Pharmacodynamic Evaluation of Novel Anticancer Agents, ON01910.Na (Rigosertib, Estybon) and ON013105, for Brain Tumor Chemotherapy. Pharm Res. 2012
33. Irizarry RA, Hobbs B, Collin F, Beazer-Barclay YD, Antonellis KJ, Scherf U, et al. Exploration, normalization, and summaries of high density oligonucleotide array probe level data. Biostatistics. 2003; 4:249–64. [PubMed: 12925520]
34. Subramanian A, Kuehn H, Gould J, Tamayo P, Mesirov JP. GSEA-P: a desktop application for Gene Set Enrichment Analysis. Bioinformatics. 2007; 23:3251–3. [PubMed: 17644558]
35. Sjoblom T, Jones S, Wood LD, Parsons DW, Lin J, Barber TD, et al. The consensus coding sequences of human breast and colorectal cancers. Science. 2006; 314:268–74. [PubMed: 16959974]
36. Clague MJ, Urbe S, de Lartigue J. Phosphoinositides and the endocytic pathway. Experimental cell research. 2009; 315:1627–31. [PubMed: 18977347]
37. Sequist LV, Heist RS, Shaw AT, Fidias P, Rosovsky R, Temel JS, et al. Implementing multiplexed genotyping of non-small-cell lung cancers into routine clinical practice. Ann Oncol. 2011; 22:2616–24. [PubMed: 22071650]

38. Adzhubei IA, Schmidt S, Peshkin L, Ramensky VE, Gerasimova A, Bork P, et al. A method and server for predicting damaging missense mutations. Nature methods. 2010; 7:248–9. [PubMed: 20354512]
39. Levine DA, Bogomolniy F, Yee CJ, Lash A, Barakat RR, Borgen PI, et al. Frequent mutation of the PIK3CA gene in ovarian and breast cancers. Clinical cancer research: an official journal of the American Association for Cancer Research. 2005; 11:2875–8. [PubMed: 15837735]
40. Reddy MV, Venkatapuram P, Mallireddigari MR, Pallela VR, Cosenza SC, Robell KA, et al. Discovery of a clinical stage multi-kinase inhibitor sodium (E)-2-{2-methoxy-5-[(2′,4′,6′-trimethoxystyrylsulfonyl)methyl]phenylamino}acetate (ON 01910.Na): synthesis, structure-activity relationship, and biological activity. J Med Chem. 2011; 54:6254–76. [PubMed: 21812421]
41. Qiu W, Schonleben F, Li X, Ho DJ, Close LG, Manolidis S, et al. PIK3CA mutations in head and neck squamous cell carcinoma. Clinical cancer research: an official journal of the American Association for Cancer Research. 2006; 12:1441–6. [PubMed: 16533766]
42. Keysar, SB.; Astling, DP.; Anderson, RT.; Vogler, BW.; Bowles, DW.; Morton, JJ., et al. A patient tumor transplant model of squamous cell cancer identifies PI3K inhibitors as candidate therapeutics in defined molecular bins. Molecular Oncology. 2013. http://dx.doi.org/10.1016/j.molonc.2013.03.004
43. Molinolo AA, Amornphimoltham P, Squarize CH, Castilho RM, Patel V, Gutkind JS. Dysregulated molecular networks in head and neck carcinogenesis. Oral Oncol. 2009; 45:324–34. [PubMed: 18805044]
44. Loi S, Michiels S, Baselga J, Bartlett JM, Singhal SK, Sabine VS, et al. PIK3CA Genotype and a PIK3CA Mutation-Related Gene Signature and Response to Everolimus and Letrozole in Estrogen Receptor Positive Breast Cancer. PloS one. 2013; 8:e53292. [PubMed: 23301057]
45. Soeda H, Shimodaira H, Watanabe M, Suzuki T, Gamoh M, Mori T, et al. Clinical usefulness of KRAS, BRAF, and PIK3CA mutations as predictive markers of cetuximab efficacy in irinotecan- and oxaliplatin-refractory Japanese patients with metastatic colorectal cancer. International journal of clinical oncology/Japan Society of Clinical Oncology. 2012
46. Hilton J, Weberpals J, Lorimer I, Amin S, Islam S, Pelletier L, et al. BRCA1 protein levels and PIK3CA mutations as predictive biomarkers for response to neoadjuvant chemotherapy in locally advanced breast cancer: An exploratory analysis. Oncology letters. 2012; 4:141–5. [PubMed: 22807977]
47. Ma WW, Messersmith WA, Dy GK, Weekes CD, Whitworth A, Ren C, et al. Phase I study of Rigosertib, an inhibitor of the phosphatidylinositol 3-kinase and Polo-like kinase 1 pathways, combined with gemcitabine in patients with solid tumors and pancreatic cancer. Clinical cancer research: an official journal of the American Association for Cancer Research. 2012; 18:2048–55. [PubMed: 22338014]
48. Bowles DW, Diamond J, Lam E, Messersmith WA, Weekes C, Leong S, et al. Phase 1 Study of Oral Rigosertib in Patients with Advanced Solid Tumors. J Clin Oncol. 2012; 30S:Abstract 3017.
49. Hsiao JR, Leu SF, Huang BM. Apoptotic mechanism of paclitaxel-induced cell death in human head and neck tumor cell lines. Journal of oral pathology & medicine: official publication of the International Association of Oral Pathologists and the American Academy of Oral Pathology. 2009; 38:188–97. [PubMed: 19200178]
50. Singh B, Reddy PG, Goberdhan A, Walsh C, Dao S, Ngai I, et al. p53 regulates cell survival by inhibiting PIK3CA in squamous cell carcinomas. Genes & development. 2002; 16:984–93. [PubMed: 11959846]
51. Yarbrough WG, Whigham A, Brown B, Roach M, Slebos R. Phosphoinositide kinase-3 status associated with presence or absence of human papillomavirus in head and neck squamous cell carcinomas. International journal of radiation oncology, biology, physics. 2007; 69:S98–101.
52. Adams JR, Xu K, Liu JC, Agamez NM, Loch AJ, Wong RG, et al. Cooperation between Pik3ca and p53 mutations in mouse mammary tumor formation. Cancer research. 2011; 71:2706–17. [PubMed: 21324922]
53. Jimeno, ABD.; Aisner, D.; Diamond, J.; Lam, E.; Weekes, C.; Leong, S.; Gore, L.; Freas, E.; Eckhardt, SG.; Messersmith, WA.; Garcia-Varella, M.; Wilhelm, F. Phase 1 and Molecular Correlates Study of Oral Rigosertib in Patients with Refractory Metastatic Head and Neck Cancer

and Advanced Solid Tumors. 104th American Association for Cancer Research (AACR) Annual Meeting, Oral presentation abstr LB-198; April 2013;

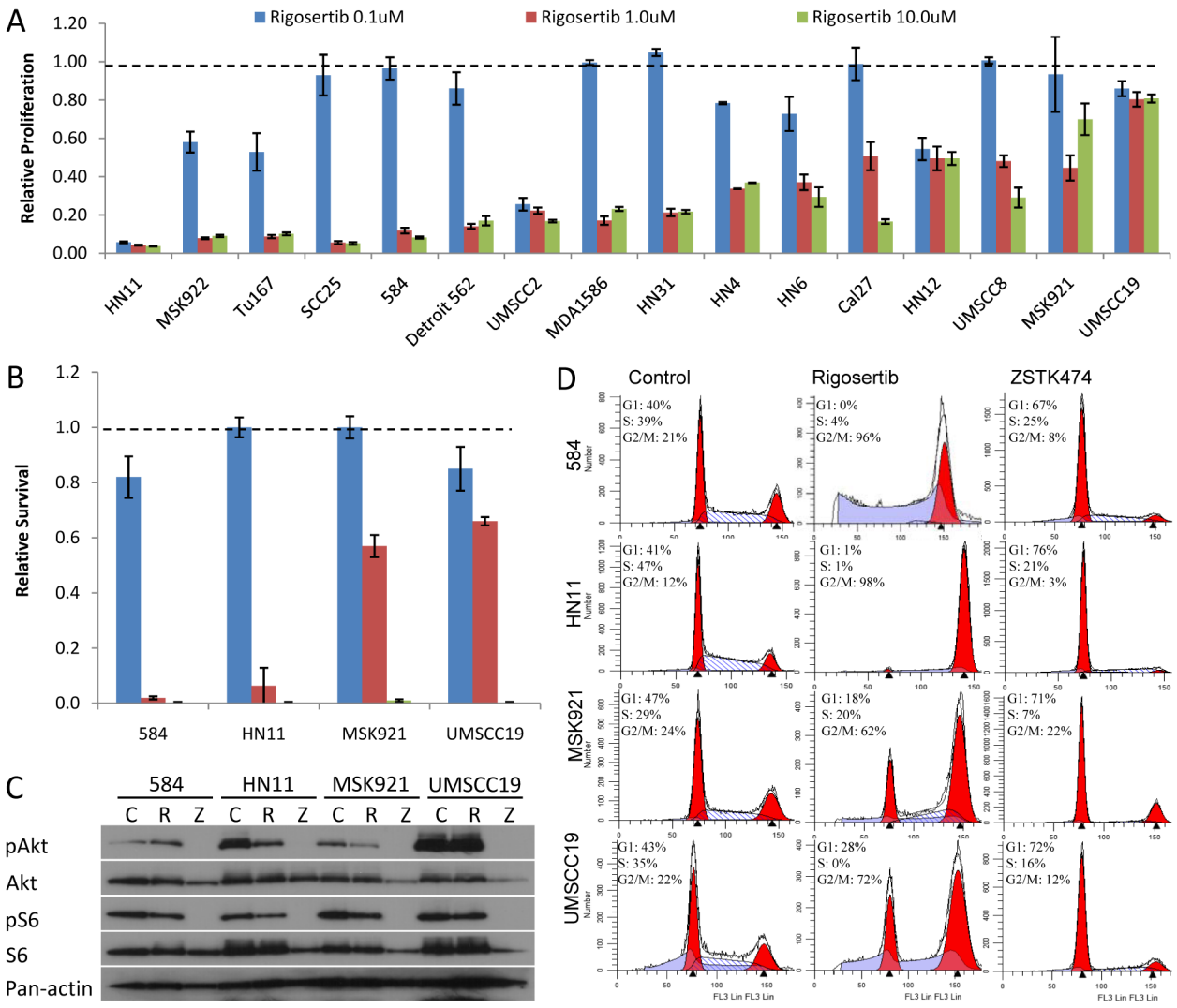

Figure 1.

A, Treated cultures (N=6) were normalized to the vehicle control data for each cell line which was set at 1.0. Cellular viability of 16 HNSCC cell lines as measured by SRB assay at 0.1uM, 1.0uM, and 10.0uM concentrations are represented graphically. Rigosertib is a potent antiproliferative agent at 1.0 μM and 10.0 μM. B, Viability of 2 sensitive (584 and HN11) and the 2 most resistant (MSK921 and UMSCC19) cell lines verified by clonogenic assay at 0.1 μM and 1.0 μM. Treatment at 10.0 μM prevented colony formation in all cell lines. C, Differential Akt and S6 phosphorylation patterns associated with treatment were identified by western blot analysis in vehicle control (C), rigosertib(R), and the PI3K inhibitor ZSTK474 (Z) treated cell culture. PI3K pathway inhibition by rigosertib is inconsistent. D, Representative cell cycle distribution by flow cytometry with ModFit analysis after 24hrs treatment with 1.0μM rigosertib or 1.0μM ZSTK474. The percentage of gated cells in each stage of the cell cycle is associated with each representative graph. Rigosertib treatment induces a pronounced G2 block in the sensitive lines. ZSTK474 induced a G1 block in all cell lines.

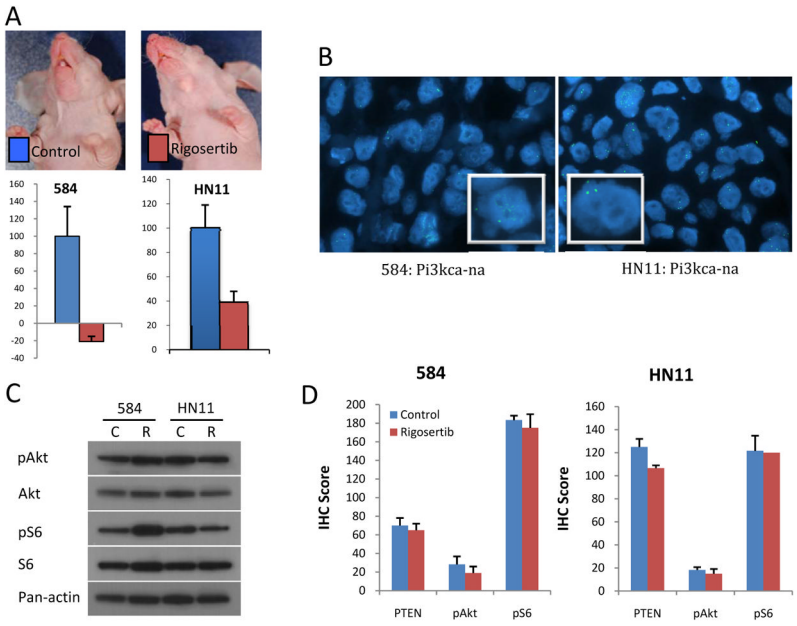

Figure 2.

A, Mice bearing orthotopically implanted cell line xenograftsof our two sensitive cell lines received daily rigosertib infusions or vehicle for 28 days. Volumes on the final day of treatment are represented as % normalized to the vehicle control group. Regression was observed in 584, and growth reduction was observed for HN11 treated tumors. B, FISH with a probe specific for *PIK3CA* showed neither engrafted cell line to have significantly increased gene copy number. C, Western blot analysis suggests rigosertib treatment moderately inhibits PI3K pathway activation in only the HN11 tumors. D, IHC scores plotted for each xenografted cell line from the control and rigosertib treated tissue of PI3K pathway endpoints confirms PI3K/Akt pathway response to rigosertib treatment.

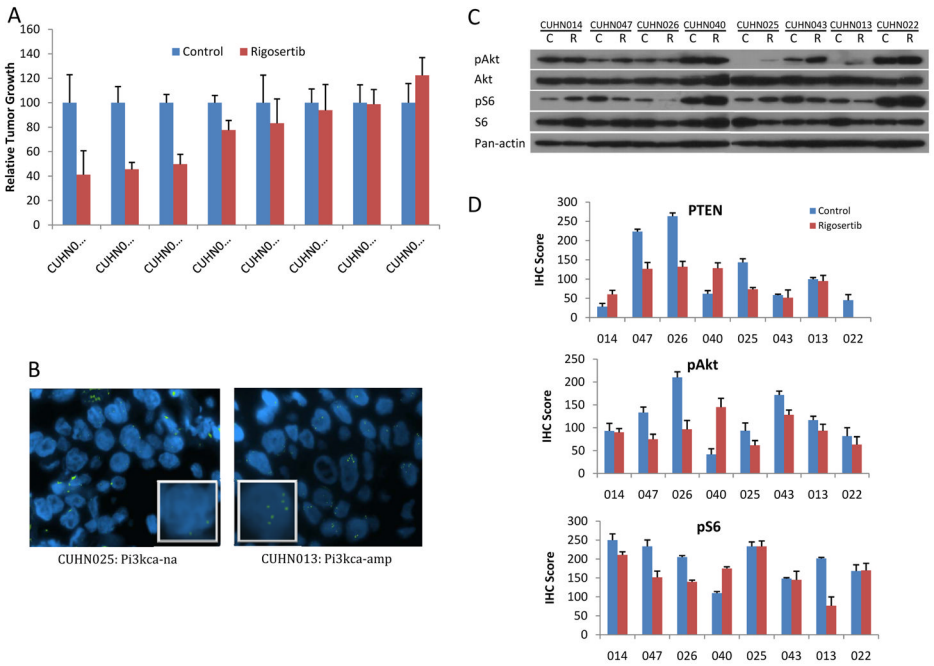

Figure 3.

A, Mice bearing patient derived tumors received daily rigosertib infusions or vehicle for 28 days. An asterisk denotes HPV16 positivity. Volumes on the final day of treatment are represented as % normalized to the vehicle control group. Growth reduction was identified in CUHN014, CUHN047 and CUHN026. B, Gene amplification was characterized by a FISH score above 4 as exemplified by CUHN013. C, Western blot analysis of tissue taken at 28-days treatmentshow inconsistent inhibition of the PI3K pathway in the vehicle control (C) and rigosertib (R) treated tissue. Inhibition of S6 phosphorylation is observed in CUHN047, CUHN026 and CUHN013. D, IHC scores plotted for each tumor line from the control and rigosertib treated tissue. The graphical representations show a correlation all sensitive lines have a decrease in S6 phosphorylation in the treated tissue. This is also true for CUHN013.

Table 1

GSEA Pathways Enriched in Resistant Cell Lines

	Gene Set Details	Key Pathways	NES	NOM p-val	FDR q-val
KEGG	KEGG_UBIQUITIN_MEDIATED_PROTEOLYSIS	Ubiquitin	−1.456	0.007	0.231
	KEGG_PROTEASOME	Proteasome	−1.468	0.035	0.232
	KEGG_PANCREATIC_CANCER	PI3K, MAPK, VEGF, p53, TGFβ	−1.557	0.009	0.143
	KEGG_DNA_REPLICATION	DNA replication	−1.573	0.015	0.145
	KEGG_SPLICEOSOME	Spliceosome	−1.820	0.000	0.044
Biocarta	BIOCARTA_MPR_PATHWAY	MAPK	−1.640	0.007	0.207
	BIOCARTA_TNFR1_PATHWAY	Apoptosis	−1.670	0.010	0.184
	BIOCARTA_PTDINS_PATHWAY	PI3K, PI	−1.680	0.003	0.189
	BIOCARTA_ETC_PATHWAY	ETC	−1.680	0.022	0.208
	BIOCARTA_FREE_PATHWAY	Apoptosis	−1.690	0.025	0.212
	BIOCARTA_BARRESTIN_SRC_PATHWAY	Endocytosis, MAPK	−1.710	0.017	0.219
	BIOCARTA_HER2_PATHWAY	Her2, MAPK	−1.810	0.000	0.123
	BIOCARTA_BARRESTIN_PATHWAY	Endocytosis	−1.870	0.006	0.111
	BIOCARTA_PROTEASOME_PATHWAY	Proteasome	−1.980	0.000	0.056
	BIOCARTA_BARR_MAPK_PATHWAY	Endocytosis, MAPK	−2.000	0.000	0.064
	BIOCARTA_EIF_PATHWAY	Translation	−2.010	0.000	0.118

Mol Cancer Ther. Author manuscript; available in PMC 2014 October 01.

Table 2

Genetic Abnormalities in HNSCC Cell Lines

Tumor Line	HPV16	*PIK3CA* Mutation	PolyPhen Prediction	PolyPhen Score	Predicted Impact	*TP53* Mutation	PolyPhen Prediction	PolyPhen Score	Predicted Impact	SNaPshot
584	-	None	-	-	-	None	-	-	-	wt
HN11	-	None	-	-	-	None	-	-	-	wt
MSK921	-	None	-	-	-	C569T (P191L) Heterozygous 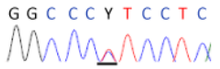	Probably Damaging	0.962	Inactivating	wt
						T695C (I232T) Heterozygous 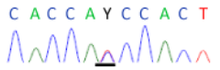	Possibly Damaging	0.725	Inactivating	
UMSCC19	-	A3140G (H1047R) Homozygous 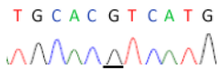	Benign	0.085	Activating	None	-	-	-	*PIK3CA* H1047R Homozygous

Table 3

Genetic Abnormalities in the Direct Patient Xenograft Tumor Lines

Tumor Line	HPV16	*PIK3CA* Mutation		PolyPhen Prediction	PolyPhen Score	Predicted Impact	*TP53* Mutation		PolyPhen Prediction	PolyPhen Score	Predicted Impact	SNaPshot
CUHN014	+	None		-	-	-	None		-	-	-	wt
CUHN047	+	None		-	-	-	N one		-	-	-	wt
CUHN026	–	G1633A (E545K) Heterozygous	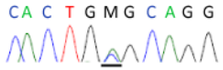	Possibly Damaging	0.868	Activating	G13371T (G245V) Homozygous	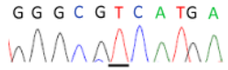	Probably Damaging	0.999	Inactivating	*PIK3CA* E545K Heterozygous
CUHN040	–	None		-	-	-	None		-	-	-	wt
CUHN025	–	None		-	-	-	G13371T (G245V) Heterozygous	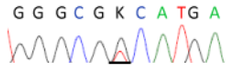	Probably Damaging	0.999	Inactivating	wt
CUHN043	+	None		-	-	-	None		-	-	-	wt
CUHN013	–	None		-	-	-	G13777A (G266E) Heterozygous		Probably Damaging	0.998	Inactivating	wt
CUHN022	+	None		-	-	-	None		-	-	-	wt